Electronic Supplementary Information

Morphology-tunable WMoO nanowires catalysts for the extremely efficient elimination of tetracycline: kinetics, mechanisms and intermediates

Yi Hu, ‡[a, c] Ke Chen,‡[b, c] Yu-Lian Li,[a, c] Jun-Yong He,[a, c] Kai-Sheng Zhang,[a] Tao Liu,[a, c] Wei Xu,[d] Xing-Jiu Huang,[a] Ling-Tao Kong*[a] and Jin-Huai Liu[a]

[a] Nano-Materials and Environmental Detection Laboratory, Institute of Intelligent Machines, Chinese Academy of Sciences, Hefei 230031, People's Republic of China.

[b] Institute of Plasma Physics, Chinese Academy of Sciences, Hefei 230031, People's Republic of China

[c] Department of Chemistry, University of Science and Technology of China, Hefei, Anhui 230026, PR China.

[d] Institute of Solid State Physics, Chinese Academy of Sciences, Hefei 230031, People's Republic of China.

‡ These two authors contributed equally to this work.

Corresponding Author

*E-mail address: ltkong@iim.ac.cn (L. Kong),

Fax: +86-551-65592420,

Tel.: +86-551-65591142.

Contents

S1. Table S1

The formulas of different samples

Samples	$C_{(NH_4)Mo_7O_{24}\cdot 4H_2O}$ (mmol/L)	$C_{H_4SiW_{12}O_{40}\cdot 7H_2O}$ (mmol/L)	$C_{C_2H_5NO_2}$ (mmol/L)	$C_{C_6H_{15}NO_3}$ (mmol/L)	Reaction Temp(°C)
WMoO-1	10	8	5	0	180
WMoO-2	10	8	5	5	180
WMoO-3	10	8	5	10	180

S2. Table S2

The amounts of each element and chemical formulas of the WMoO-*x* (*x* = 1, 2 and 3) determined by ICP-MS and XRD technologies.

Samples	Mo (μg/mL)	W (μg/mL)	Mo/W (atomic %)	XRD Model	Chemical Formulas
WMoO-1	27.42	36.22	1.451	$Mo_{17}O_{47}$ $WO_{2.72}$	$WMo_{1.45}O_{6.72}$
WMoO-2	30.55	38.78	1.511		$WMo_{1.51}O_{6.89}$
WMoO-3	26.73	30.19	1.697		$WMo_{1.70}O_{7.41}$

S3. Figure S1. XRD spectra of the as-prepared WMoO-*x* (*x* = 1, 2 and 3) catalysts.

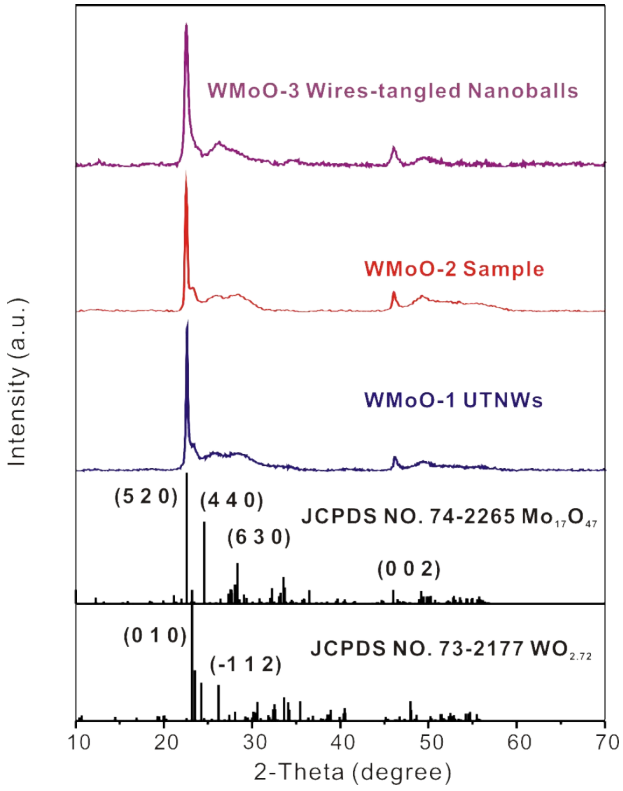

S4. Figure S2. N_2 adsorption-desorption isotherms and BJH adsorption pore size distribution of the mixed-valence WMoO-*x* (*x* = 1, 2 and 3) catalysts.

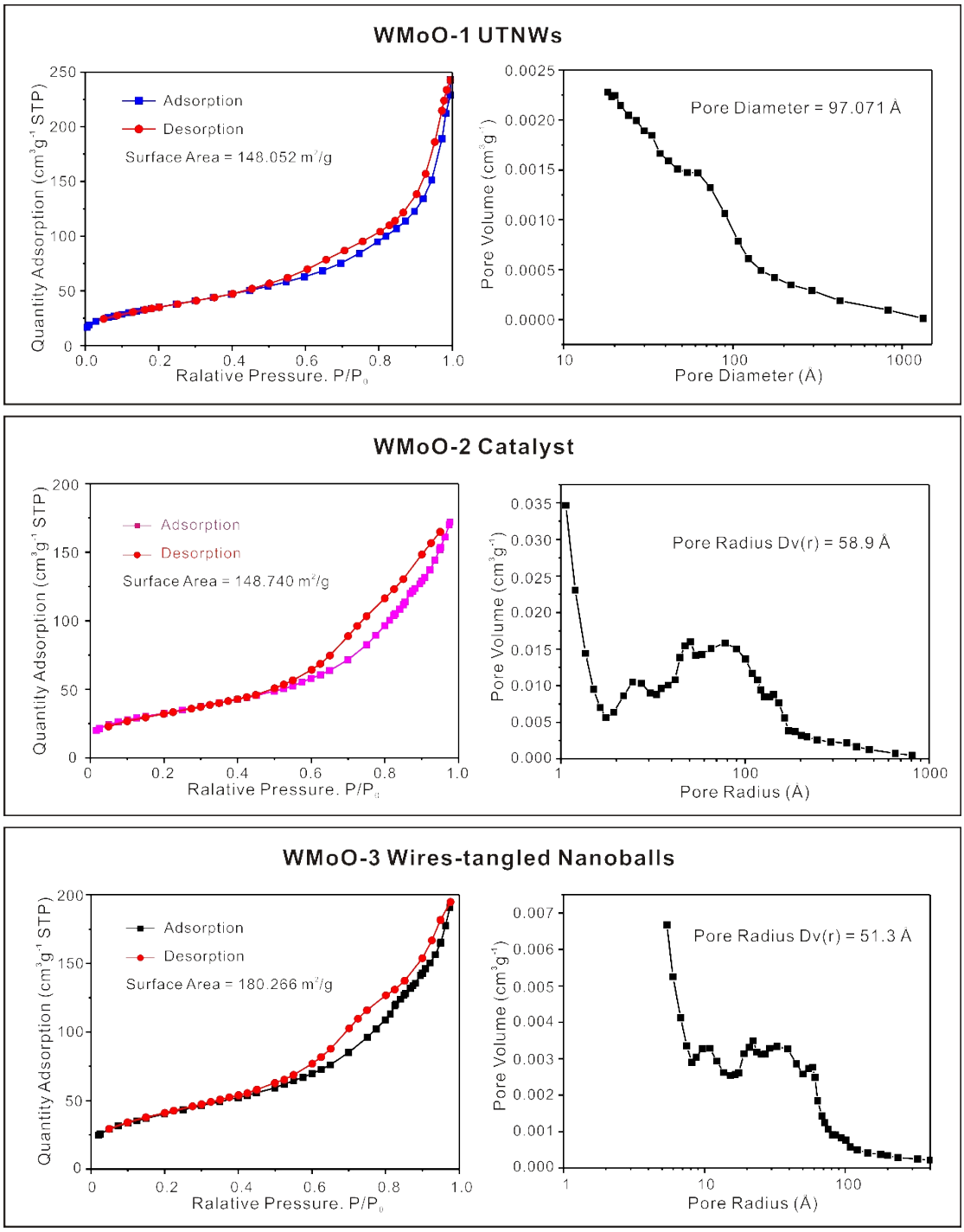

S5. Figure S3. SEM (A1-A3), TEM (B1-B3) EDS (C1-C3 and D) and AFM (E1, E2) images of the WMoO-1 UTNWs.

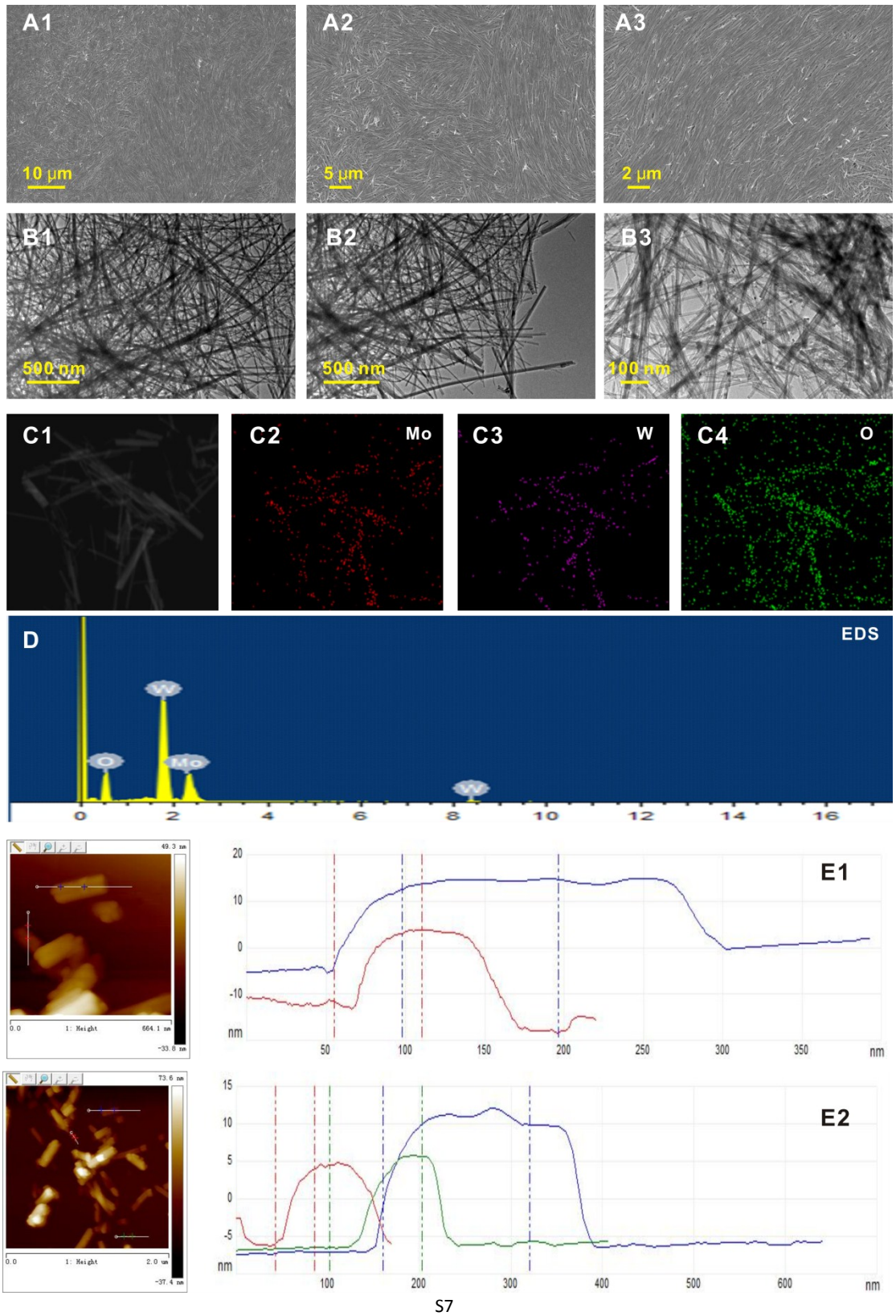

S6. Figure S4. The SEM and TEM spectra of (A) WMoO-2 and (B) WMoO-3 wires-tangled nanoballs.

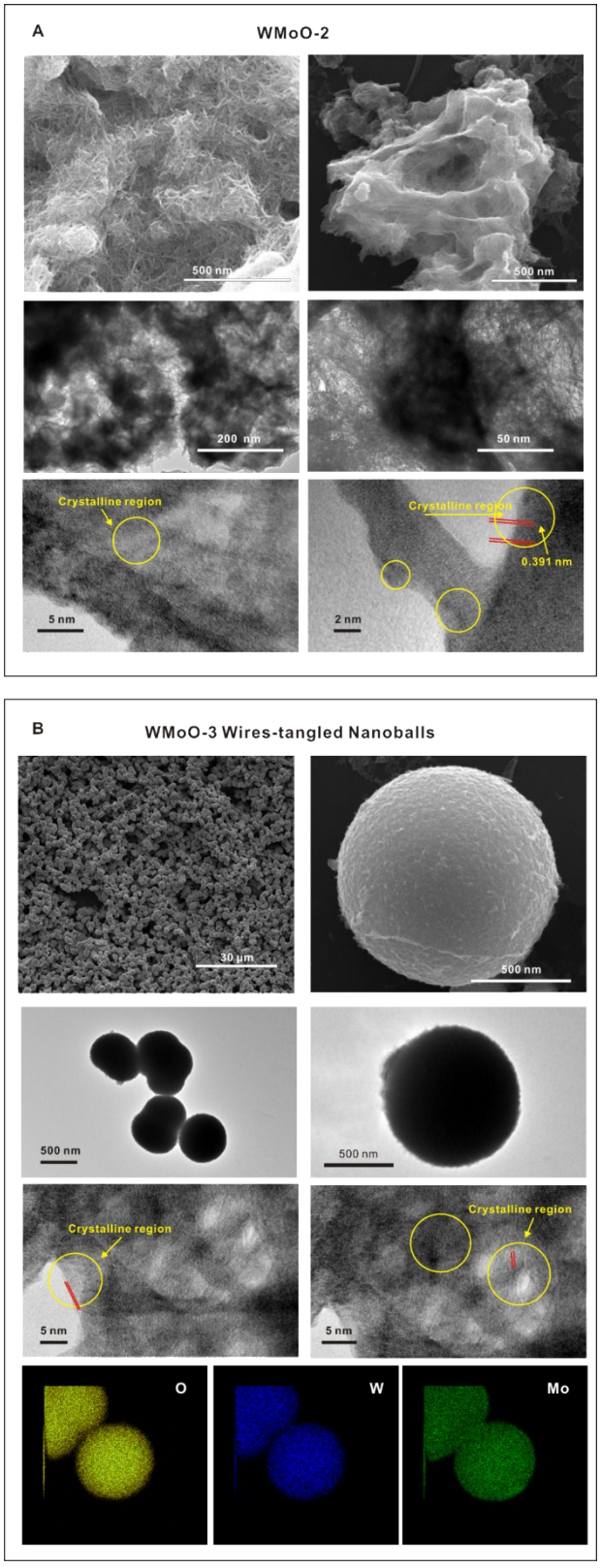

S7. Figure S5. XPS spectra of the mixed-valence WMoO-*x* (*x* = 1, 2 and 3) catalysts.

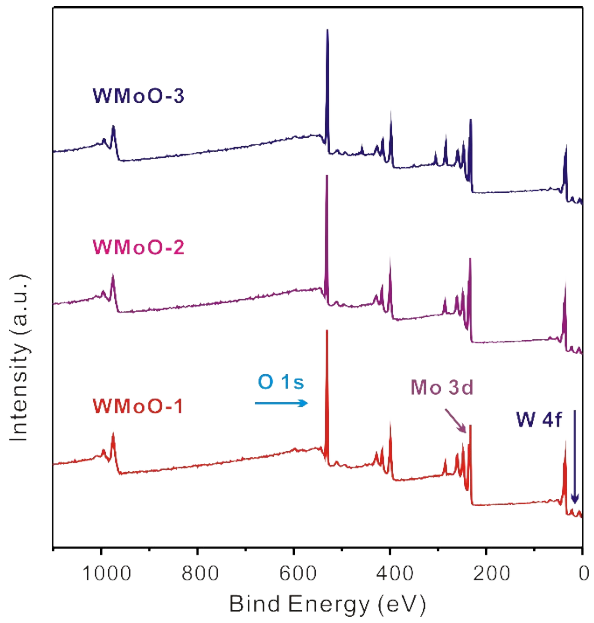

S8. More details and illustrations about ·OH and unpaired electrons detection by use of EPR technology

Detection of unpaired electrons:

Variable temperature EPR spectra of the WMoO-*x* samples were obtained using a JEOL JES-FA 200 EPR spectrometer (140 K, 9.058GHz, X-band). Microwave power employed was 1 mW; sweep width ranged from 223 to 423 mT. Modulation frequency and modulation amplitude were 100 kHz and 0.35 mT, respectively.

Detection of hydroxyl radicals (·OH):

As a matter of fact, hydroxyl radicals and superoxide radicals are always present in the Fenton-like oxidation system. However, the oxidative potential of hydroxyl radicals is higher than that of superoxide radicals. And the superoxide radicals are more difficult to detect than hydroxyl radicals in aqueous systems. Therefore, the signal of ·OH is normally used as a measure to evaluate the performance of a wide variety of Fenton-like systems.

In oxidation-relevant systems, ·OH is often produced in the course of a Fenton-like reaction occurring upon decomposition of H_2O_2 as follows:

$$M^{(n+1)+} + H_2O_2 \rightarrow MOOH^{n+} + H^+ \qquad (1)$$

$$MOOH^{n+} \rightarrow M^{n+} + HO_2^{\cdot} \qquad (2)$$

$$M^{n+} + H_2O_2 \rightarrow M^{(n+1)+} + OH^- + \cdot OH \qquad (3)$$

While the short-lived ·OH radicals cannot be directly detected by electron paramagnetic resonance (EPR) because of their very short lifetime and low steady-state concentrations, they would readily react with diamagnetic nitrone spin trap

dimethyl pyridine N-oxide (DMPO), forming a stable free radical (spin adduct) that could be identified based on the magnetic parameters of the EPR spectrum. So DMPO was employed in this study to detect the existence of ·OH.

The wave spectrogram contains a free radical spectrum composed of a four-line EPR signal with a 1:2:2:1 peak to peak pattern and the isotropic hyperfine coupling constants ($A_N = A_H \approx 14.9$ G) that are characteristic of the DMPO-·OH adduct.

S9. Figure S6. EPR spectra of ·OH collected with different WMoO-*x* (*x* = 1, 2 and 3) catalysts. Reaction condition: WMoO-*x* dosage = 0.8 g/L, $[H_2O_2]_0$ = 20 mM, $[DMPO]_0$ = 100 mM. All the spectra were obtained 10 min after mixing, neutral condition and 25 °C.

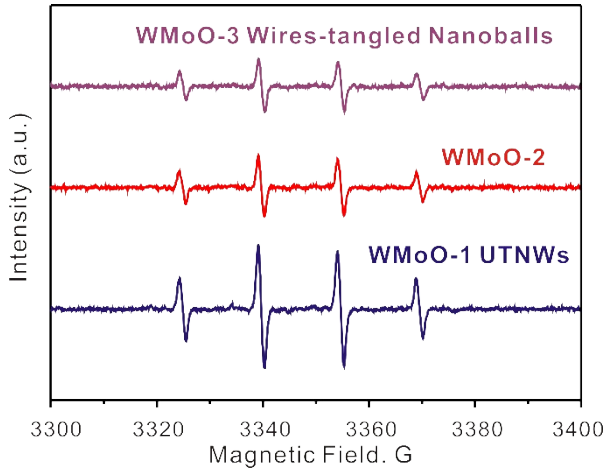

S10. The synthetic route of $W_{18}O_{49}$.

In brief, 50 mg of WCl_6 was initially dissolved in to 35 ml ethanol solution, which was vigorously stirred for 60 min to prepare a transparent light-yellow solution. Then it was transferred into a 50 ml PFA-lined autoclave and heated under autogenously temperature at 200 °C for 12 h and cooled to room temperature (RT). The resultant product was separated by centrifugation, and washed with anhydrous ethanol for several times. Finally, the obtained powders were freeze-drying at -40 ^{o}C for whole night for further use.

S11. Figure S7. FTIR spectra of the mixed-valence WMoO-*x* (*x* = 1, 2 and 3) catalysts.

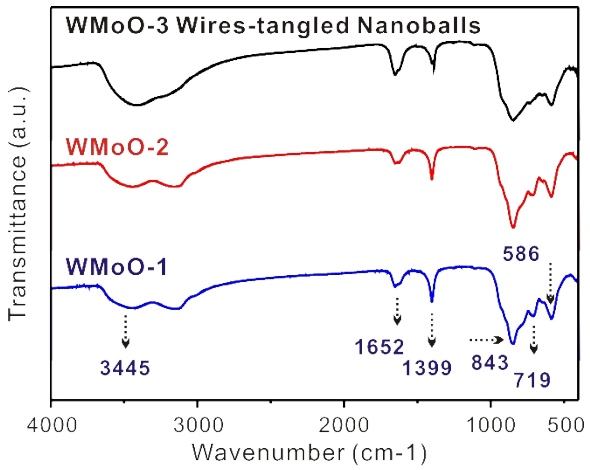

S12. Figure S8. TGA analysis of the mixed-valence WMoO-*x* (*x* = 1, 2 and 3) catalysts.

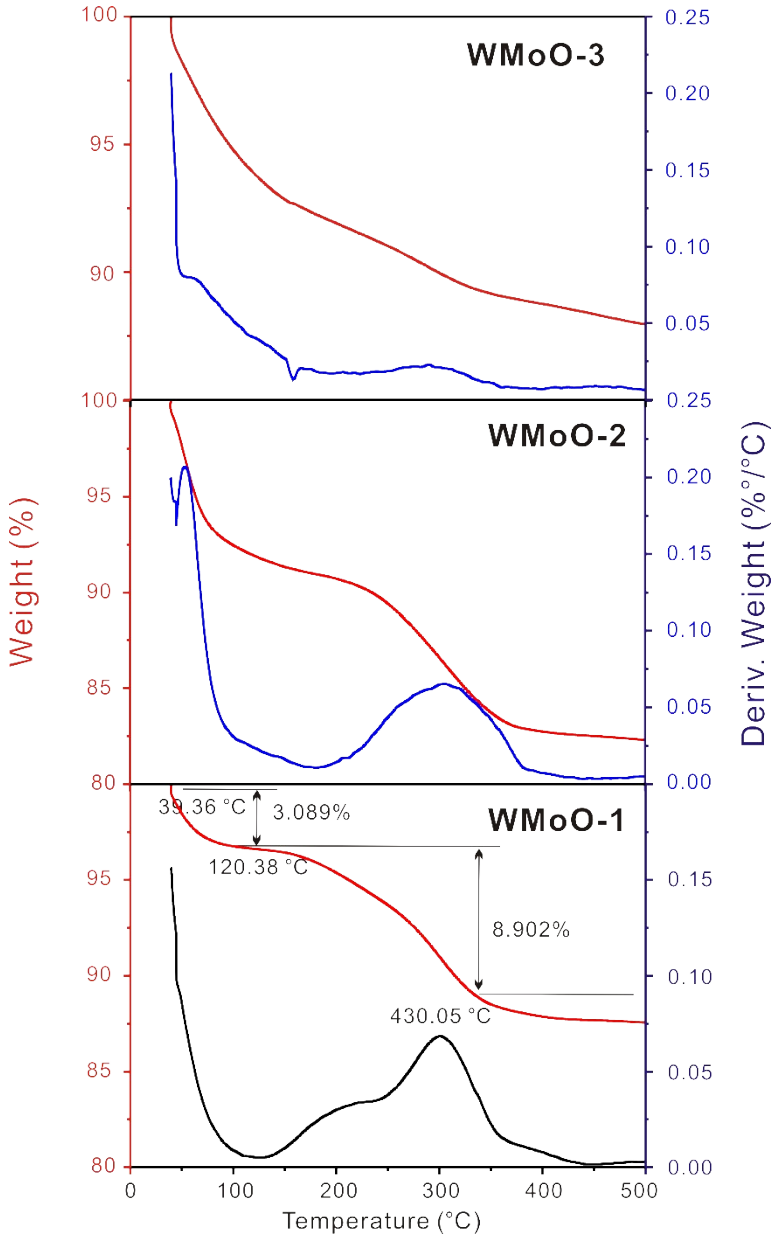

S13. Figure S9. The adsorption behaviors of TC on the WMoO-*x* (*x* = 1, 2 and 3) catalysts. $[TC]_0$ = 10 mg/L, WMoO-*x* dosage = 1 g/L, t = 25 °C, neutral condition.

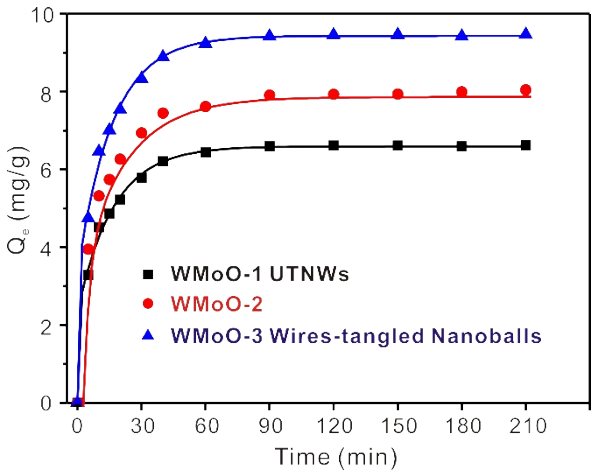

Figure S9 demonstrates the adsorption behaviors of TC on the WMoO-1, WMoO-2 and WMoO-3 catalysts. It is significant that the WMoO-3 wires-tangled nanoballs had the best adsorption performance among the three samples, nearly 95% of TC was removed in 90 min, which could attribute to the more adsorption sites provided by its lager surface area. The as-prepared material of WMoO-3 wires-tangled nanoballs could be used as adsorbent for extremely efficient removal of low concentrations of TC in a short time.

S14. Figure S10. The degradation behaviors of TC on $W_{18}O_{49}$ and WMoO-*x* (*x* = 1, 2 and 3) catalysts. Reaction condition: $[TC]_0$ = 400 μM, WMoO-*x* dosage = 0.8 g/L, $[H_2O_2]_0$ = 20 mM, pH = 3, t = 25 °C.

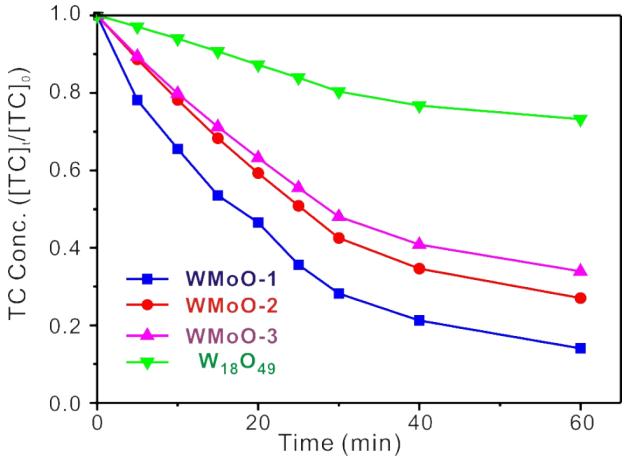

Figure S10 depicts the degradation bahaviors of TC on $W_{18}O_{49}$, WMoO-1, WMoO-2 and WMoO-3 catalysts. WMoO-1 UTNWs displayed the best catalysis in degradation of TC among these three catalysts.

Compare with the $W_{18}O_{49}$ sample, the WMoO-1 catalyst showed the excellent performance on degradation of TC, which could be attributed to efficiently catalyze H_2O_2 generating ·OH and elevate the defect-band central towards Fermi level.

Compare with the WMoO-1 UTNWs (Fig. 1D), it could be found that WMoO-2 (Figure S4A) and WMoO-3 WTNBs (Figure S4B) failed to meet a better crystallinity, although the surface areas of these samples were larger (Figure S2). It's generally believed that a large specific surface area could improve the adsorption performance and thereby increase the activity of a catalyst. But it's often unavailable when increase the specific surface area at the expense of active surface. Therefore, the results could

attribute to that the great crystallinity and the ultrathin nanowires structure of WMoO-1 UTNWs exposes more active surface used for the degradation of TC.

S15. Figure S11. LC-MS spectrum of TC degradation during the WMoO-1/H_2O_2 Fenton-like process.